Effect of plate permeability on nonlinear stability of the asymptotic suction boundary layer

Håkan Wedin,[1,*] Stefania Cherubini,[2] and Alessandro Bottaro[1]

[1]*Department of Civil, Chemical and Environmental Engineering, University of Genova, Via Montallegro 1, 16145 Genova, Italy*
[2]*DynFluid, Arts et Métiers ParisTech, 151 Boulevard de l'Hôpital, 75013 Paris, France*

The nonlinear stability of the asymptotic suction boundary layer is studied numerically, searching for finite-amplitude solutions that bifurcate from the laminar flow state. By changing the boundary conditions for disturbances at the plate from the classical no-slip condition to more physically sound ones, the stability characteristics of the flow may change radically, both for the linearized as well as the nonlinear problem. The wall boundary condition takes into account the permeability $\hat{K}$ of the plate; for very low permeability, it is acceptable to impose the classical boundary condition ($\hat{K} = 0$). This leads to a Reynolds number of approximately $\text{Re}_c = 54\,400$ for the onset of linearly unstable waves, and close to $\text{Re}_g = 3200$ for the emergence of nonlinear solutions [F. A. Milinazzo and P. G. Saffman, J. Fluid Mech. **160**, 281 (1985); J. H. M. Fransson, Ph.D. thesis, Royal Institute of Technology, KTH, Sweden, 2003]. However, for larger values of the plate's permeability, the lower limit for the existence of linear and nonlinear solutions shifts to significantly lower Reynolds numbers. For the largest permeability studied here, the limit values of the Reynolds numbers reduce down to $\text{Re}_c = 796$ and $\text{Re}_g = 294$. For all cases studied, the solutions bifurcate subcritically toward lower Re, and this leads to the conjecture that they may be involved in the very first stages of a transition scenario similar to the classical route of the Blasius boundary layer initiated by Tollmien-Schlichting (TS) waves. The stability of these nonlinear solutions is also investigated, showing a low-frequency main unstable mode whose growth rate decreases with increasing permeability and with the Reynolds number, following a power law $\text{Re}^{-\rho}$, where the value of ρ depends on the permeability coefficient $\hat{K}$. The nonlinear dynamics of the flow in the vicinity of the computed finite-amplitude solutions is finally investigated by direct numerical simulations, providing a viable scenario for subcritical transition due to TS waves.

PACS number(s): 47.27.Cn, 05.45.−a, 47.85.Dh

I. INTRODUCTION

The motion of a fluid is generally characterized as being in a laminar or turbulent condition. The state in between those two, the transitional state, usually has large fluctuations in pressure and shear stress due to an alternation between laminar and turbulent flow. To achieve a dynamical system description of the turbulent transition, one needs insight on the behavior of exact coherent solutions to the Navier-Stokes equations, such as simple traveling waves (TWs) and complex periodic orbits. The study of finite-amplitude TWs provides a good illustration of how a flow may bifurcate from a well-ordered laminar flow to a nonlinear state. These waves have been shown to have some relevance to the actual transition process; for instance, simple two-dimensional Tollmien-Schlichting (TS) waves have proved to be a part of the early stage of the transition process in the Blasius boundary layer flow in a low-disturbance environment [1]. When they are of large enough amplitude, they go through a secondary instability that brings the flow to turbulence [2]. Secondly, the signature of three-dimensional (3D) traveling waves in Ref. [3] and the observation of a mechanism that sustains them in Ref. [4] has provided convincing evidence that numerically obtained *exact coherent structures* (ECSs) can be good candidates for obtaining a theoretically grounded view of turbulence. The regeneration cycle presented in Ref. [5] can be used to discover self-sustained three-dimensional traveling waves to the incompressible Navier-Stokes equations [6–8]. TWs

satisfying $\boldsymbol{u}_t = -c\boldsymbol{u}_x$, propagating at constant wave speed c without altering their shape, have now been discovered for many canonical shear flows. Examples of previous work include plane Poiseuille flow [9], plane Couette flow [10,11], the Blasius boundary layer flow [12,13], pipe flow [14,15], and the asymptotic suction boundary layer flow [16]. The square duct configuration has been studied less, but it has been shown to possess traveling waves of various shapes [17–20]. The intriguing aspect of the TWs is their innate unstable nature (see, e.g., [20]), which renders them interesting flow objects to account for in a dynamical system description of turbulence. Although the global traveling waves appear to resemble turbulent flow structures, they do not capture the bursting flow phenomenon, i.e., the breakup and recreation of exact coherent structures, and they are not localized in the streamwise direction, as observed particulary in pipe flow. A more recent approach and the next step in the hierarchy of solutions, capable of revealing turbulent dynamics, are recurrent time-dependent periodic orbits that may be extracted from numerical simulations [21–29] or through a bifurcation from a global traveling wave [30]. However, the entanglement of the stable and unstable manifold of the TWs, which can be viewed as saddle points in a reference moving with the base flow, creates the potential for subcritical transition and consequent turbulence sustainment. Thus, investigating the TWs dynamics might be crucial to unravel the nonlinear dynamics of shear flows that are prone to subcritical transition, such as the asymptotic suction boundary layer. In fact, although for this flow the critical Reynolds number appears to be very high, namely $\text{Re}_c \approx 54\,382$ [31], the amplitude thresholds for the subcritical transition are very low, and they scale

———————
*hakanwedin@hotmail.com

as Re^{-2}, as recently found in Ref. [32] using a nonlinear optimization coupled with a bisection procedure in order to find the minimal-energy perturbation able to induce subcritical transition in such a flow. Such a subcritical transition scenario is characterized by inclined streamwise vortices and strongly bent streaks, able to rapidly bypass the asymptotic growth of TS waves. Previous investigations of TWs in the asymptotic suction boundary-layer flow have been performed in Ref. [16], neglecting the influence of the permeability of the flat plate on the development of the perturbations. This hypothesis, which has been used in most of the linear and nonlinear stability analyses concerning this flow, might have an effect on the determination of its stability thresholds, which appears to be overpredicted with respect to experimental observations [33].

This paper presents two-dimensional traveling-wave solutions of the Navier-Stokes equations for the asymptotic suction boundary layer configuration. The original side of the results presented herein is the physically sound condition imposed for the disturbance velocity at the plate, which differs from the classical no-slip boundary condition used elsewhere. Linear stability results and nonlinear finite-amplitude solutions will be provided, focusing on the two-dimensional case, in order to provide a thorough comparison with the linear and nonlinear critical Reynolds numbers available in the literature. The paper is organized as follows: In Sec. II, we present the flow configuration and the equations. In Sec. III, the finite-amplitude solutions are presented together with a three-dimensional stability analysis and their role in phase space. Finally, conclusions can be found in Sec. IV.

II. DEFINITIONS

Two-dimensional nonlinear solutions in the asymptotic suction boundary layer have already been presented in [16], with vanishing disturbance velocity at the porous plate. The original aspect in the present work is the imposition of a condition for the velocity through the plate derived using Darcy's law; this leads to a drastic change in the stability characteristics of the laminar flow. The streamwise, vertical, and spanwise coordinates are represented by $\hat{x}$, $\hat{y}$, and $\hat{z}$; the unit vectors are **i**, **j**, and **k** used for defining the velocity vector $\hat{\boldsymbol{u}} = \hat{u}\mathbf{i} + \hat{v}\mathbf{j} + \hat{w}\mathbf{k}$ referring to the streamwise, wall-normal, and spanwise component, respectively; $\hat{p}$ stands for pressure, $\hat{v}$ and $\hat{\mu}$ are the kinematic and dynamic viscosity, respectively, and time is $\hat{t}$. The dimensional laminar base state with no pressure gradient imposed is $\hat{\boldsymbol{U}}(\hat{y}) = \hat{U}(\hat{y})\mathbf{i} + \hat{V}\mathbf{j}$. The solution of $\hat{U}$ can be found in [34] and is

$$\hat{U}(\hat{y}) = \hat{U}_\infty[1 - \exp(-\hat{V}_0\hat{y}/\hat{v})], \qquad (1)$$

$$\hat{V} = -\hat{V}_0 = \text{const}, \qquad (2)$$

where the wall-normal component $\hat{V}_0 > 0$ is constant over a large area as opposed to a mere local action of the suction. As in earlier studies, a uniform suction $\hat{V}_0$ is assumed to be maintained through the plate; in an experimental setup, the porous medium is composed of voids of finite size, hence the suction is not exactly uniform (see the sketch in Fig. 1). However, if the pore size and spacing between pores are sufficiently small, the wall-normal suction can be considered
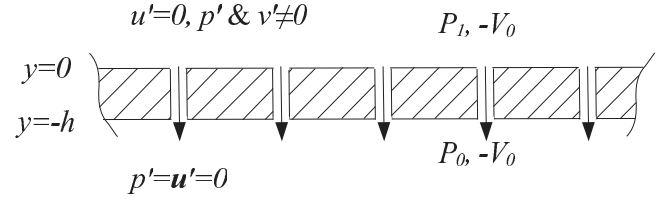

FIG. 1. A schematic of the plate showing the main idea behind the imposed boundary conditions at $y = 0$. Variables in capital letters refer to the base flow.

uniform over a *representative elementary volume* that is large on the pore scale. Thus, the flow components in Eqs. (1) and (2) characterize a type of boundary-layer flow that does not vary in the streamwise direction; this solution is approached when uniform suction is applied for a sufficiently long distance from the beginning of the suction zone, resulting in the analytical solution given in Eqs. (1) and (2).

The Navier-Stokes equations are nondimensionalized (thus the caret symbols are removed) using the streamwise free-stream speed $\hat{U}_\infty$ at the outer edge of the computational domain $\hat{y} = \hat{y}_\infty$, density $\hat{\rho}$, and the displacement thickness $\hat{\delta}_*$, so that the Reynolds number is defined as $Re = \hat{U}_\infty\hat{\delta}_*/\hat{v}$. The governing equations are the Navier-Stokes equations and the continuity equation:

$$\boldsymbol{u}_t + \boldsymbol{u} \cdot \nabla\boldsymbol{u} + \nabla p - \frac{1}{Re}\nabla^2\boldsymbol{u} = \mathbf{0}, \qquad \nabla \cdot \boldsymbol{u} = \mathbf{0}. \quad (3)$$

To search for two-dimensional nonlinear solutions, we perform a bifurcation study in which we add a perturbation to the base state $\boldsymbol{U}(y)$, yielding the total flow $\boldsymbol{u} = \boldsymbol{U}(y)\mathbf{i} + V\mathbf{j} + \epsilon\boldsymbol{u}'$, where ϵ is an amplitude to be determined. The nondimensional laminar flow is $U(y) = 1 - e^{-y}$ and $V = -1/Re$. Substituting for $\boldsymbol{u}$ in the Navier-Stokes and continuity equations, and subtracting the base flow equations, leads to the disturbance equations. Since the base flow depends only on y, we impose periodicity in x and t for $\boldsymbol{u}'$ representing the solution as a traveling wave,

$$\boldsymbol{u}' = \sum_b \boldsymbol{u}^{(b)}(y)\exp[ib\alpha(x - ct)], \qquad (4)$$

where $b = -NX, \ldots, +NX$, α is a real streamwise wave number, and $c = c_r + ic_i$ is in general a complex eigenvalue to be determined ($i = \sqrt{-1}$). The Fourier amplitude $\boldsymbol{u}^{(b)}(y)$ is expressed in a Chebyshev series with $NY + 1$ polynomials T_i, where $\boldsymbol{u}^{(-b)} = \boldsymbol{u}^{*(b)}(y)$ (∗ denotes complex conjugate). The above solution of $\boldsymbol{u}'$, for a monochromatic wave, grows/decays and oscillates in time with growth rate αc_i and frequency αc_r. The wall-normal flow domain is truncated from $[0,\infty)$ to the computational domain $[0, y_\infty]$ and then transformed to the interval $[-1, +1]$ in γ using the formula $y = a(1 + \gamma)/(b - \gamma)$, where $a = y_i y_\infty/(y_\infty - 2y_i)$, $b = 1 + 2a/y_\infty$, where y_i is the distance from the plate where half of the collocation points sit. The equations are imposed on the Gauss-Lobatto grid distribution, $\gamma_k = \cos(k\pi/NY)$, for $k = 0, 1, 2, \ldots, NY$. To ensure a uniform free-stream flow $\boldsymbol{u}(y = y_\infty) = (1, -1/Re)$, also in the presence of finite-amplitude perturbations, we impose Fourier modes decaying exponentially as $y \to \infty$. To comply with the uniform flow condition, we set $v^{(b=0)} = 0$. At

the plate, the streamwise disturbance velocity is assumed to vanish, i.e., $u'(t,x, y = 0) = 0$; however, due to the fact that the wall is porous, it is not obvious that the v' component of the perturbation should be zero, as customarily assumed in most linear and nonlinear studies [16,26,27,35–39]. For low permeabilities, it is acceptable to represent the flow through the porous plate via Darcy's law, neglecting inertia, i.e.,

$$\hat{\boldsymbol{u}} = -(\hat{K}/\hat{\mu})\hat{\nabla}\hat{p}, \qquad (5)$$

under the assumption that the porous medium is isotropic so that $\hat{K}$ is a scalar parameter. Typically, the permeability $\hat{K}$ ranges from 2×10^{-17} m^2 for concrete to 10^{-6} m^2 for some metal foams [40], a function of the porosity and the structure of the medium. Following Gustavsson [35], we consider a dimensional flow given by $(-\hat{V}_0 + \hat{v}', \hat{P}_1 + \hat{p}')$ at $\hat{y} = 0$ and the unperturbed state $(-\hat{V}_0, \hat{P}_0)$ at $\hat{y} = -\hat{h}$, with $\hat{h}$ the plate's thickness (see Fig. 1). In dimensionless terms, Darcy's law for the disturbance at $y = 0$ becomes

$$v' = -ap', \qquad (6)$$

with $a = \hat{U}_\infty \hat{K}/(\hat{v}\hat{h})$ the dimensionless permeability parameter. We limit the range of $\hat{K}$ to an upper value of 2×10^{-9} m^2 for Darcy's law to be tenable (for larger permeabilities, the Forchheimer model is a better representation of the relation between the pressure gradient and the average velocity through the porous medium). Using the data of Fransson and Alfredsson [33] ($\hat{U}_\infty = 5$ ms^{-1}, $\hat{v} = 1.5 \times 10^{-5}$ m^2 s^{-1}, $\hat{h} = 3.2$ mm), we thus have

$$0 \leqslant a \leqslant 0.2;$$

the gas permeability of the porous plastic plate used in [33] has been measured to be 3.7×10^{-12} m^2, which translates to a dimensionless value $a = 3.85 \times 10^{-4}$, to be later used as a reference.

Subtracting the x derivative of the streamwise momentum equation from the y derivative of the normal momentum equation, both taken at the wall, using continuity and the relation $v' = -ap'$, we finally obtain the wall condition for v':

$$\frac{v'_{xx} - v'_{yy}}{2a} + \epsilon v'v'_{yy} - \frac{v'_{yy} + v'_{yyy}}{\text{Re}} = 0, \qquad (7)$$

which, in a linearized setting, using the Fourier series in (4), translates to

$$\left[\frac{a}{\text{Re}}(D^3 + D^2) + \frac{1}{2}(D^2 + \alpha^2)\right]v = 0,$$

with $v = v^{(1)}(y)$ the first mode of the vertical velocity component in Eq. (4) and $D = d/dy$. The recent linear stability study by Pluvinage *et al.* [41] adopts a condition equivalent to the one given above, whereas the present nonlinear contribution employs the full equation (7).

To give a measure of the amplitude of the nonlinear wave, we compute the energy E of the x-dependent part:

$$E = \frac{1}{2}\epsilon^2 \int_0^{2\pi/\alpha} \int_0^{2\pi/\beta} \int_0^{y_\infty} [u'^2 + v'^2 + w'^2]dX\,dy\,dz, \qquad (8)$$

where X corresponds to the time-independent Galilean frame $X = x - c_r t$. For the two-dimensional TS waves, we have $w' = 0$. Finally, the linear and nonlinear dynamics of the

computed TWs has been analyzed by using direct numerical simulation (DNS) in a three-dimensional framework. A computational box with dimensions $L_x \times L_y \times L_z = 4\pi/\alpha \times y_\infty \times 2\pi$ is considered, and y_∞ is the same as the one chosen for computing the TWs. In this computational domain, the Navier-Stokes equations, written in a perturbative formulation, are discretized and solved using a finite-difference fractional-step method with second-order accuracy in space and time [42]. In the wall-normal direction, the grid distribution given by the mapping of the Gauss-Lobatto points in the $[0, y_\infty]$ domain has been kept. Concerning the streamwise and spanwise directions, equally spaced grid points have been used. The number of grid points in each direction has been chosen after careful validation of the reference domain $20\pi \times 40 \times 2\pi$. For instance, this domain has been discretized by a grid made by $201 \times 121 \times 61$ grid points. Concerning the boundary conditions, at the wall the nondimensional Darcy law for the wall-normal perturbations given in Eq. (6) is imposed, whereas a zero perturbation condition is used for the streamwise and spanwise velocities as well as for all of the perturbation components at the upper boundary. In the spanwise and streamwise direction, periodicity is imposed for the three velocity components. For each value of Re, α, y_∞, and a, the simulations have been initialized by superposing to the base flow the TW solution for the streamwise and wall-normal velocity components; the perturbation of this relative fixed point has been initialized by a random zero-mean noise of amplitude 10^{-8} for the spanwise velocity component, multiplied by an envelope function that smoothly brings it to zero toward the wall. This three-dimensional velocity component allows the most unstable mode of the TW to develop more quickly. Both the linear and nonlinear time evolution of the perturbations have been studied, the former by neglecting the perturbative nonlinear terms in the Navier-Stokes equations, the latter by considering the whole equations.

III. RESULTS

The core of the results presented herein revolves around the fact that modifying the wall conditions of v' to the physically based slip condition (7) leads to a dramatic change of the stability of the flow. To bring the solutions into the nonlinear regime, we locate a vanishing imaginary part of the eigenvalue c ($c_i = 0$) in parameter space resolving the linearized governing equations. We then search for a bifurcation to obtain a nonlinear wave with wave speed c_r. For this, a FORTRAN subroutine utilizing a Newton-Raphson technique is used, developed in [43,44]. For $c = c_r$, a time-independent problem can be considered in a Galilean frame of reference (or $x - c_r t \rightarrow X$) moving with the wave speed c_r. The solutions presented in Fig. 2 show the envelope of the perturbation energy E over Re for $\alpha = 0.154$ and various values of the nondimensional permeability a. The solution with the classical vanishing disturbance velocities at the wall (i.e., $a = 0$) corresponds to the study presented in Ref. [16] and is close to the case $a = 3.85 \times 10^{-4}$ of the wind tunnel experiments by Fransson and Alfredsson [33]. For $a = 0$ it is remarkable that when reducing the Re from more than 50 000 to around 5000–6000, a very low perturbation energy
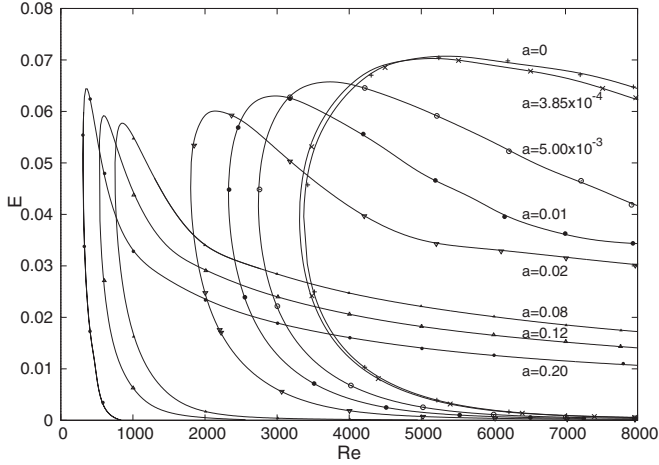
FIG. 2. The energy E of the wavy part of the nonlinear solutions, see Eq. (8), mapped out in Re for a streamwise wave number of $\alpha = 0.154$ and eight values of a. The classical wall condition $a = 0$ corresponds to a bifurcation at $\text{Re}_c \approx 54\,000$ for $\alpha_c = 0.1555$ [16,36]. With increasing a, Re_c is reduced. This is also the case for the nonlinear lower limit, cf. Table I. Proof of convergence is shown by the individual symbols; for $a < 0.02$ we use as a base resolution $(NX, NY) = (14, 140)$ and confirmed with $(18, 160)$. The $a = 0.02$ solution is mapped out using a truncation of $(10, 160)$ and confirmed with $(14, 200)$, while the $a = 0.08$, 0.12 and 0.20 solutions are represented by a resolution of $(14, 200)$ and confirmed with $(18, 220)$.

is sufficient to bring the flow to a new flow state, as shown in Fig. 2, in agreement with the results in Ref. [32]. When increasing the value of a, a striking change is observed in the bifurcation diagram; progressively lower values of the
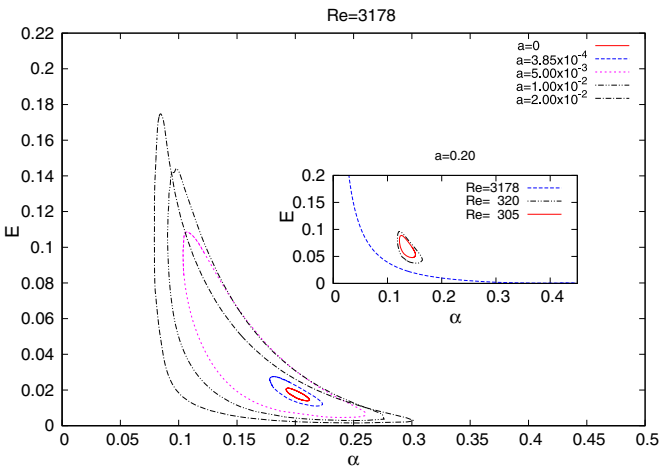

FIG. 3. (Color online) Perturbation energy E of the wavy part mapped out in α for $a = 0$ (22,100), 3.85×10^{-4} (26,120), 5×10^{-3} (18,160), 0.01 (18,160), and 0.02 (14,200) at Re = 3178 (see the legends). The values in the parentheses after each value of a refer to the truncation (NX, NY) used. The selected Re lies in the neighborhood of the Re_g of the $a = 0$ solution as evidenced by its narrow envelope in α. Table I shows the values of Re_g for all a's presented in the plot. The inset shows the energy for $a = 0.20$ at Re = 305 and 320 using a truncation of $(14, 180)$ and 3178 using $(12, 240)$. The lower values of Re shown in the smaller plot are close to the limit Re_g for $a = 0.20$ given in Table I.

TABLE I. The critical Reynolds numbers Re_c and Re_g of the Tollmien-Schlichting waves for a few selected values of the nondimensional permeability a. Re_c is the critical limit for linear instability, and Re_g defines the emergence of nonlinear states. The corresponding limits of the Blasius boundary-layer flow (no suction) lie at $\text{Re}_c = 520$ and $\text{Re}_g = 510$ [12,45].

a	α_c	Re_c	α_g	Re_g
0	0.1555	54 379	0.200	3168
3.85×10^{-4}	0.155	53 171	0.205	3128
5×10^{-3}	0.160	41 492	0.185	2693
0.01	0.170	32 886	0.168	2324
0.02	0.175	22 268	0.136	1795
0.20	0.120	796	0.131	294

bifurcation point Re_c for linear stability are found, and the same goes for the lower limit where alternative nonlinear states to the Navier-Stokes equations emerge, $\text{Re} = \text{Re}_g$.

Figure 2 shows that for a low nondimensional permeability $a = 3.85 \times 10^{-4}$, the use of the classical condition ($a = 0$) is reasonable for approximating the real flow. This is better illustrated by the comparable envelope in the perturbation energy over α in Fig. 3 for $a = 3.85 \times 10^{-4}$ and $a = 0$. However, increasing a decreases the value of both Re_c and Re_g further away from the classical case of $a = 0$. The larger plot in Fig. 3 shows E of the nonlinear solutions mapped out in α as a function of a for $\text{Re} = 3178$. When $a = 0$, the envelope is very narrow since we are near Re_g. Increasing a further, one sees that for $a = 0.01$ the solutions encompass a greater range in both amplitude and wave number. According to the inset in Fig. 3 for $a = 0.20$, at $\text{Re} = 3178$ the range of α's admitted by the Navier-Stokes equations is broadened to both larger and smaller values compared to the lower-a case in the main plot at the same Reynolds number. The $a = 0.20$ solution has only one branch at $\text{Re} = 3178$ (also seen in Fig. 2) as opposed to two for the solutions at lower values of a. Decreasing Re further, an upper and a lower branch appear for Re lower than the bifurcation point (where $E = 0$). Moreover, the inset in Fig. 3 shows the admitted streamwise wave numbers for $a = 0.20$ as a function of Re, down to values close to its Re_g. Moving in α-Re parameter space, one finds the lower limits in Re of the linear and the finite amplitude solutions
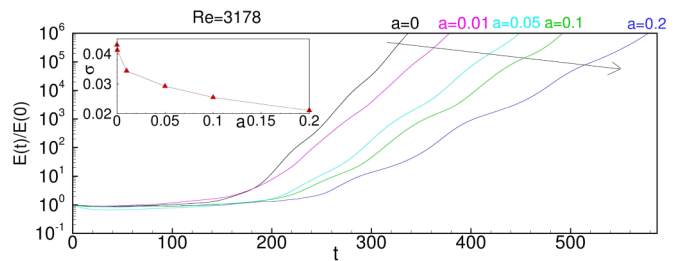

FIG. 4. (Color online) Energy growth extracted from a linearized three-dimensional DNS initialized with several nonlinear Tollmien-Schlichting waves. The solutions selected are the upper branch ones with $\alpha = 0.20$ and Re = 3178 (see Fig. 3). The inset shows the growth rate σ for several values of a ranging from 0 to 0.2, whereas the main plot shows the time evolution of the three-dimensional energy for $a = 0$, 0.01, 0.05, 0.1, and 0.2.
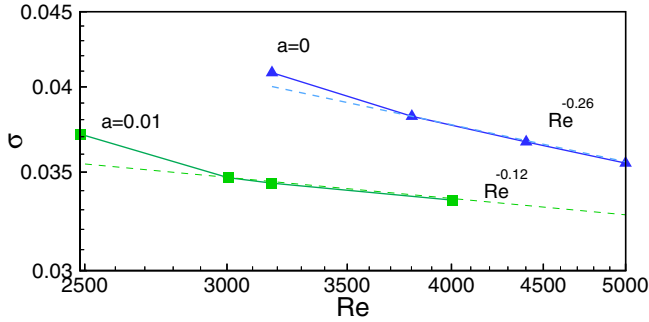
FIG. 5. (Color online) Variation with Re of the growth rate σ of the unstable mode for the upper branch TWs with $\alpha = 0.20$, $a = 0$ (blue), and $a = 0.01$ (green). The scaling law is represented by a dashed line.

given in Table I. In particular, Re_c changes from 54 379 (for $a = 0$) to 796 (for $a = 0.2$), whereas Re_g changes from 3168 to 294. Notice that in the case with $a = 0$, the perturbation at the wall is set to zero, whereas homogeneous suction is still present in the base flow. Thus, the critical Reynolds numbers found for $a = 0$ cannot be compared to those of the Blasius boundary layer (i.e., $Re_c = 520$ and $Re_g = 510$ [12,45]), but rather with the ones provided in the literature for the asymptotic suction boundary layer with no-slip boundary conditions for the disturbance velocity, namely $Re_c \approx 54\,400$ and $Re_g \approx 3200$ [16,36]. Concerning the case with $a = 3.85 \times 10^{-4}$, one can notice that the predicted critical Reynolds number and streamwise wave number are in good agreement with the ones provided by Fransson and Alfredsson [33] (i.e., $Re_c = 54\,382$ and $\alpha_c = 0.1555$).

Investigating the stability of these solutions is crucial to characterize their dynamics; thus, we have performed linearized DNSs initialized by several upper branch TW solutions selected for different a values at $Re = 3178$ and $\alpha = 0.2$ (close to the saddle-node bifurcation for $a = 0$; see Fig. 3). The plot in Fig. 4 provides the time evolution of the energy integrated

in the three-dimensional computational domain, showing that for $t > 200$, an asymptotically increasing trend exists for all of the considered solutions. These curves change only slightly for increasing spanwise domains, meaning that the unstable mode has a wavelength that is contained in the 2π domain. The main unstable mode is characterized by a low temporal frequency ($\omega \approx 0.06$ for $a = 0.2$) and a growth rate, σ, which decreases with an increase of a, as shown by the red triangles in the inset frame. This might seem surprising, since an increasing value of a has been previously found to increase the base flow instability; however, this behavior might be linked to the relative distance of the selected bifurcated solutions to the saddle-node bifurcation, as also observed in Ref. [46] for Couette flow. We have performed simulations at different Reynolds numbers in order to establish the dependence of the unstable mode growth rate with respect to its distance (in terms of Re) to the saddle-node bifurcation. The results are displayed in Fig. 5, which shows σ as a function of Re for two values of a, namely $a = 0$ and 0.01: except for Reynolds numbers very close to the bifurcation point, σ scales with Re following a power law, close to $Re^{-0.26}$ for $a = 0$ and $Re^{-0.12}$ for $a = 0.01$; conversely, a steepest dependence on the Reynolds number, providing an asymptotic scaling of $Re^{-0.48}$, was observed for a lower branch fixed point in the Couette flow in Ref. [46]. Thus, in the range of Reynolds number explored here, the TWs for the case of nonzero permeability are more stable than those found for $a = 0$, and this fact is of some relevance when assessing the stability of the ASBL flow. The most unstable modes together with the associated TWs are shown in Fig. 6 for the two selected values of a, $Re = 3178$ and $\alpha = 0.2$. The TW superposed to the base flow solution, shown by the colored isocontours in the $z = 2\pi$ plane, induces a streamwise modulation in the thickness of the asymptotic suction boundary-layer flow. One can observe that this modulation is stronger for a larger value of a (at the same Re), since the selected upper-branch TWs tend to have a larger amplitude for increasing a (see the envelopes in Fig. 3). The unstable mode is shown in the same figure
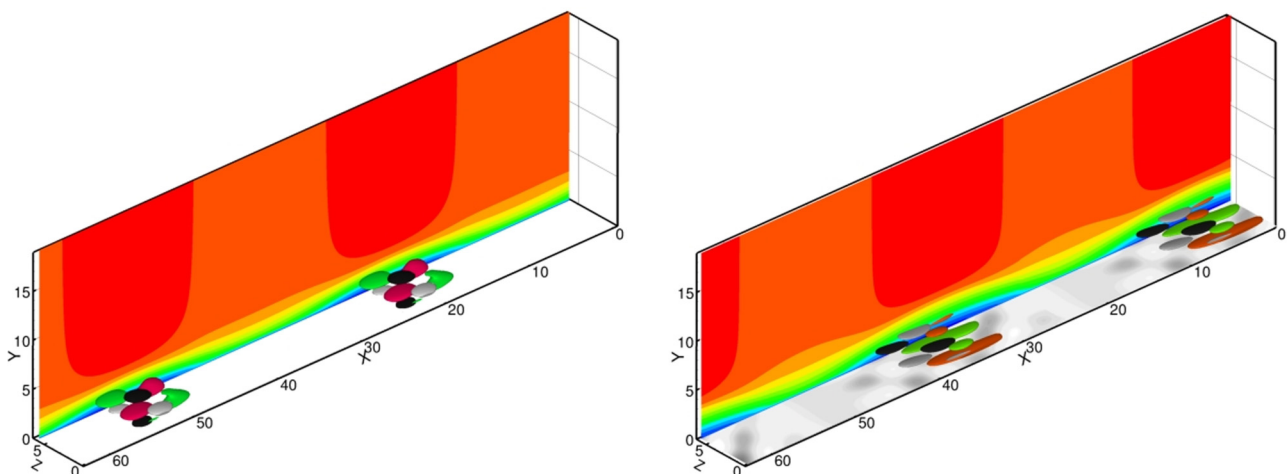

FIG. 6. (Color online) Colored isocontours of the streamwise instantaneous velocity on the plane $z = 2\pi$ and isosurfaces of the streamwise (red and green) and the spanwise (black and white) perturbation to the TW extracted at $t = 2000$ from a linearized DNS initialized by the upper branch solution with $\alpha = 0.20$, $Re = 3178$, $a = 0$ (left), and $a = 0.01$ (right). The gray isocontours in the right frame represent the wall-normal perturbation at the wall.
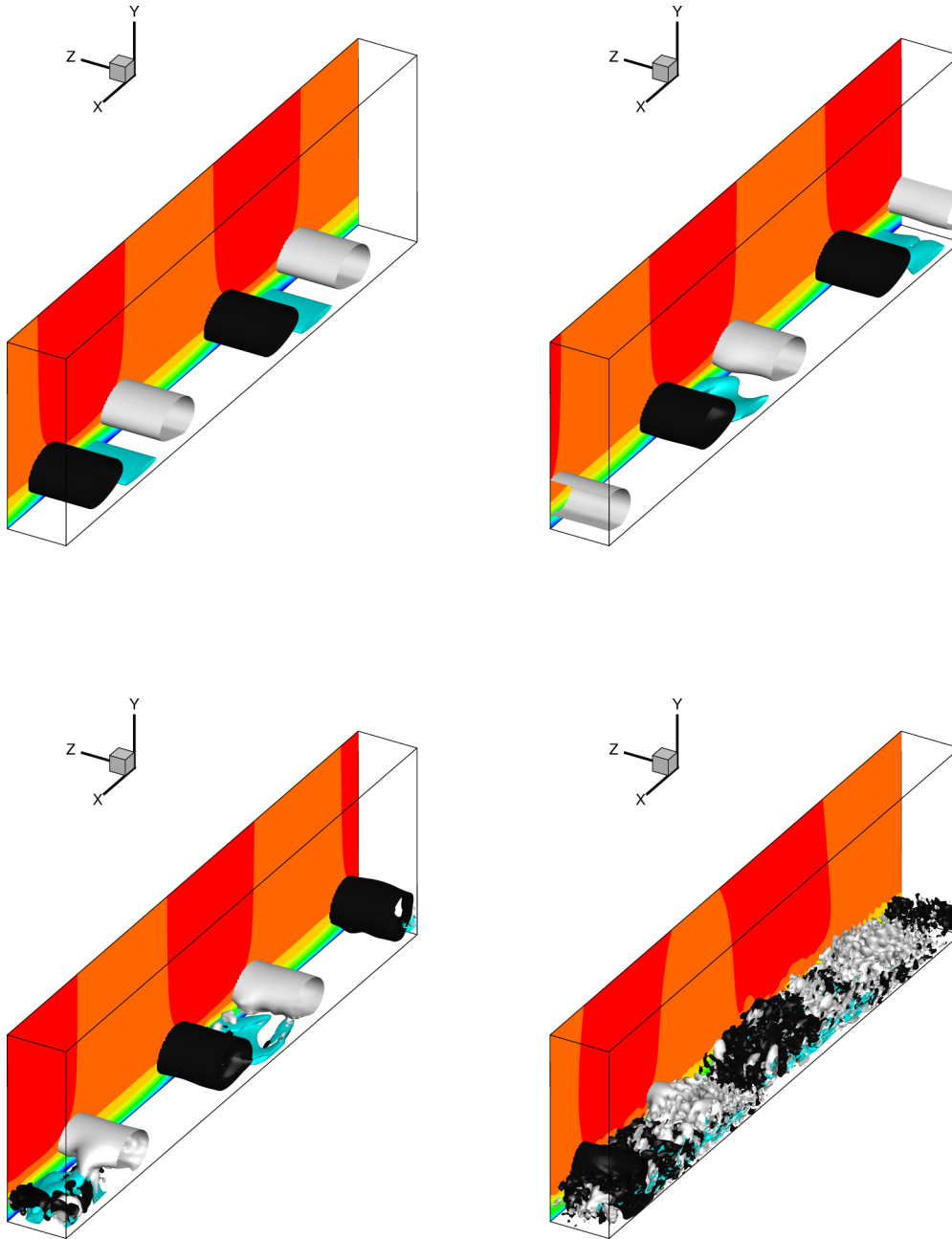
FIG. 7. (Color online) Colored isocontours of the streamwise instantaneous velocity on the plane $z = 2\pi$ and isosurfaces of the streamwise (light blue) and the wall-normal (black and white) perturbation to the base flow extracted at $t = 300, 350, 400$, and 500 (from left top to right bottom) from a DNS initialized by the upper branch solution with $\alpha = 0.20$, Re $= 3178$, and $a = 0$.

by the isosurfaces of streamwise (red for positive and green for negative) and spanwise (white for positive and black for negative) perturbation. The unstable mode is localized in the streamwise region in which the TW induces a deceleration of the flow, and it allows a three-dimensionalization of the flow structures leading the flow to transition. One can also observe that, for $a = 0.01$, the unstable mode is more elongated in the streamwise direction than for $a = 0$, probably due to the presence of a nonzero wall-normal velocity at the wall (see the gray isocontours at the wall), which may tend to induce a delocalization of the disturbance.

The destabilization of the TWs and the nonlinear dynamics of the resulting flow structures have been further investigated

by nonlinear DNS. Figure 7 provides the dynamics of the total perturbation of the base flow, $\mathbf{u} - \mathbf{U}$, for $a = 0$, Re $= 3178$, and $\alpha = 0.20$, at four different times, $t = 300, 350, 400$, and 500. The black/white and the light blue surfaces indicate wall-normal and streamwise perturbations to the base flow, respectively, whereas the colored contours represent the streamwise instantaneous velocity on the plane $z = 2\pi$. At $t = 300$ (top left frame), the perturbation still appears to be two-dimensional, maintaining the shape of the TS-wave nonlinear solution, inducing a streamwise modulation on the asymptotic suction boundary layer profile. The fact that the flow field remains very close to the nonlinear TS wave for such a long time confirms that the TW solution is characterized

by a high-dimensional stable manifold. One can notice also that, similarly to what has been observed experimentally by Fransson and Alfredsson [33] for the asymptotic suction boundary layer in the presence of TS waves, the streamwise velocity perturbation has a large-amplitude peak very close to the wall, whereas the wall-normal one is weaker and peaks farther from the wall. However, at $t \approx 350$ (top right frame), the flow structures are suddenly three-dimensionalized by the effect of the previously shown unstable mode, which induces a spanwise modulation of the perturbation. In particular, the streamwise perturbation to the base flow, which is localized in the vicinity of the wall, appears more affected by the unstable mode than the wall-normal one, which is placed at larger values of the wall-normal coordinate. At $t \approx 450$ (bottom left frame), even the flow structures placed farther from the wall begin to be affected by the growing unstable wave, displaying strong spanwise oscillations. As a consequence, the TW experiences breakdown and very rapid transition to turbulence (see the bottom right frame at $t = 500$). The trajectory of the perturbation can also be observed on an E_v-E_w projection of the state space in Fig. 8 by the red (gray) line representing the case with zero permeability, where E_w is the integrated energy of the spanwise component of the velocity perturbation, and E_v is the wall-normal one. One can see that both E_w and E_v strongly increase only after the unstable mode is triggered (the small red dot represents the flow state at $t = 300$). Then the trajectory follows the unstable manifold of the TW solution (the middle-sized red dot representing the state at $t = 400$) very rapidly increasing in both E_w and E_v, and, after having reached a peak, it begins to relax toward a statistically steady state (see the larger red dot for $t = 500$). A similar picture can be observed for a nonzero permeability, the black curve showing the trajectory for $a = 0.1$. Note that a larger peak value of E_w and E_v is reached before transition to turbulence when an increased permeability is considered, resembling a bursting phenomenon, characterized by a large increase of both the energy and the dissipation [47]. Furthermore, for $a = 0.1$, the transition occurs at larger times, as shown by the black small dot, which represents the flow state at $t = 400$, being still very close to the TW solution, as well as by the flow structures displayed in Fig. 9 for $t = 450, 500, 550,$ and 600. The route to
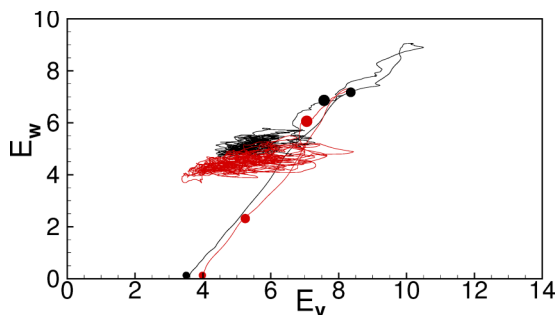
the transition is similar to the previous case, although it occurs in a larger time frame, and the streamwise perturbations appear to be more elongated in the streamwise direction. These results clearly point out the strong influence of the permeability of the flat plate on the nonlinear stability and transition to turbulence of the asymptotic suction boundary-layer flow.

IV. CONCLUSIONS

Finite-amplitude traveling wave (TW) solutions for the asymptotic suction boundary-layer flow are investigated, taking into account the permeability of the wall. Comparing with earlier results that set vanishing disturbance velocity components at the porous boundary, we show that both the linear stability limit Re_c as well as the lower limit of the nonlinear solutions Re_g change dramatically when the permeability $\hat{K}$ of the plate is accounted for, using Darcy's law. Increasing the plate permeability from zero, the linear stability limit Re_c is lowered from around 54 400 to less than 800, corresponding to the largest $\hat{K}$ examined here. Moreover, the nonlinear limit Re_g of the finite-amplitude solutions changes from 3168 to 294. For the range of permeabilities studied, this means that the asymptotic suction boundary layer has still a higher limit in Re_c compared to the Blasius boundary layer [45]. However, looking at the nonlinear limit Re_g, the solutions for the asymptotic suction case are far below the corresponding minimum point of the Blasius boundary layer [12]. Thus, wall suction appears to be stabilizing for low-amplitude perturbations, while finite-amplitude disturbances are more easily destabilized—compared to the Blasius case—provided the permeability of the porous wall, $\hat{K}$, is sufficiently large. The stability of the traveling waves is also investigated, showing a low-frequency main unstable mode whose growth rate decreases with increasing permeability, with a power-law dependence on the Reynolds number. The nonlinear dynamics of the flow in the vicinity of the computed TWs is finally investigated by direct numerical simulations, showing that the flow remains for a large time close to the TW solution; transition, however, occurs very quickly once the unstable mode is triggered, inducing a strong increase of the spanwise and wall-normal perturbations of the base flow, resembling a bursting phenomenon. The unstable mode induces a three-dimensionalization of the TW, which rapidly leads to transition, providing a relevant scenario for subcritical transition due to TS waves.

In this work, it has been shown that imposing boundary conditions that take into account the permeability of the wall may strongly affect the bifurcation curves and the stability properties of two-dimensional TW solutions. This may explain why previous theoretical stability results, obtained by neglecting wall permeability, appear to overpredict the stability of the flow with respect to experimental observations [33]. Moreover, the time evolution of the nonlinear TS waves computed here fits well the scenario of transition induced by TS waves in boundary-layer flows, where TS waves of sufficiently high amplitude (>1% of the mean streamwise velocity) are found to generate three-dimensional waves and vortices that induce the growth of chaotic hotspots [48]. This transition scenario typical of boundary-layer flows may be strongly delayed by wall suction in the case of a negligible

FIG. 8. (Color online) Flow trajectory plotted on an E_v-E_w projection of the phase space, extracted from a DNS initialized with the upper branch solutions with $\alpha = 0.20$, $Re = 3178$, $a = 0.0$ [red (gray) line], and $a = 0.1$ (black line). The red dots indicate the state at $t = 300, 400,$ and 500 (for increasing dot size), whereas the black ones indicate the state at $t = 450, 550,$ and 650 (for increasing dot size).
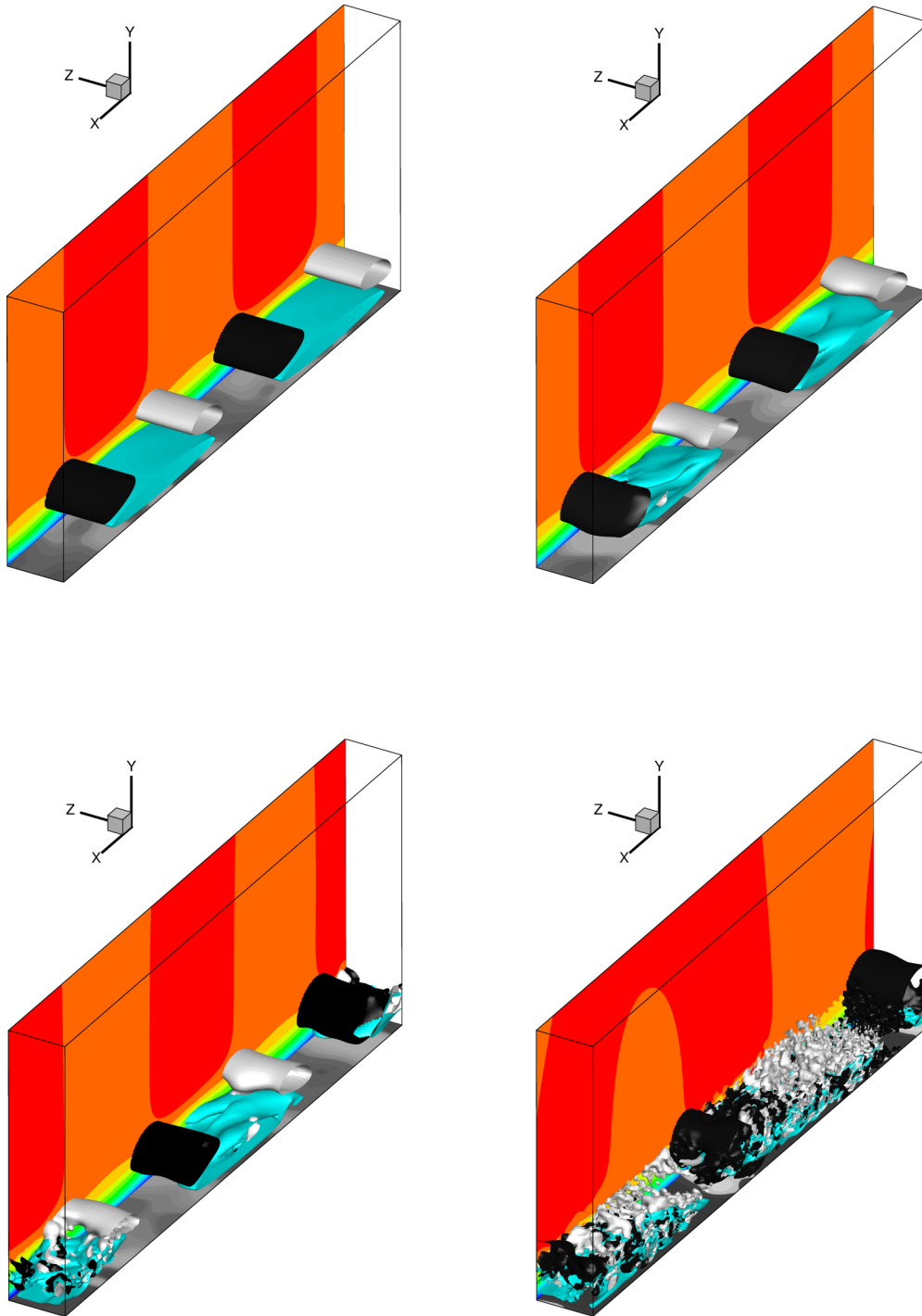
FIG. 9. (Color online) Colored isocontours of the streamwise instantaneous velocity on the plane $z = 2\pi$ and isosurfaces of the streamwise (light blue) and the wall-normal (black and white) perturbation to the base flow extracted at $t = 450, 500, 550,$ and 650 (from left top to right bottom) from a DNS initialized by the upper branch solution with $\alpha = 0.20$, Re $= 3178$, and $a = 0.1$. The gray isocontours at $y = 0$ represent the wall-normal perturbation at the wall.

wall permeability [33], since the critical Reynolds number for TS waves is found to strongly increase. However, in this work we have shown that, when wall permeability is accounted for, the critical Reynolds numbers decrease again, reaching values even lower than the ones typical of the Blasius boundary layer. Thus, the dynamics of the nonlinear TS waves can be considered representative of the transition scenarios that can be observed for moderate Reynolds numbers and non-negligible

wall permeability. Nevertheless, it is well known that the asymptotic suction boundary layer can also experience bypass transition due to the formation and secondary instability of streamwise streaks and vortices, which are inherently three-dimensional coherent structures. Thus, future works will aim at computing three-dimensional TW solutions in order to unravel the effect of the plate's permeability on the bypass transition scenario.

[1] M. Matsubara and P. Alfredsson, Disturbance growth in boundary layers subjected to free-stream turbulence, J. Fluid Mech. **430**, 149 (2001).

[2] T. Herbert, Secondary instability of boundary layers, Annu. Rev. Fluid Mech. **20**, 487 (1988).

[3] B. Hof, C. Doorne, J. Westerweel, F. Nieuwstadt, H. Faisst, B. Eckhardt, H. Wedin, R. Kerswell, and F. Waleffe, Experimental observation of nonlinear traveling waves in turbulent pipe flow, Science **305**, 1594 (2004).

[4] B. Hof, C. W. H. van Doorne, J. Westerweel, and F. T. M. Nieuwstadt, Turbulence regeneration in pipe flow at moderate Reynolds numbers, Phys. Rev. Lett. **95**, 214502 (2005).

[5] F. Waleffe, On a self-sustaining process in shear flows, Phys. Fluids **9**, 883 (1997).

[6] F. Waleffe, Three-dimensional coherent states in plane shear flows, Phys. Rev. Lett. **81**, 4140 (1998).

[7] F. Waleffe, Exact coherent structures in channel flow, J. Fluid Mech. **435**, 93 (2001).

[8] F. Waleffe, Homotopy of exact coherent structures in plane shear flows, Phys. Fluids **15**, 1517 (2003).

[9] U. Ehrenstein and W. Koch, Three-dimensional wavelike equilibrium states in plane Poiseuille flow, J. Fluid Mech. **228**, 111 (1991).

[10] M. Nagata, Three-dimensional finite-amplitude solutions in plane Couette flow: Bifurcation from infinity, J. Fluid Mech. **217**, 519 (1990).

[11] J. Gibson, J. Halcrow, and Cvitanović, Visualizing the geometry of state space in plane Couette flow, J. Fluid Mech. **611**, 107 (2008).

[12] J. Rotenberry, Finite amplitude steady waves in the Blasius boundary layer, Phys. Fluids A **5**, 1840 (1993).

[13] H. Wedin, A. Bottaro, A. Hanifi, and G. Zampogna, Unstable flow structures in the Blasius boundary layer, Eur. Phys. J. E **37**, 34 (2014).

[14] H. Wedin and R. Kerswell, Exact coherent structures in pipe flow: travelling wave solutions, J. Fluid Mech. **508**, 333 (2004).

[15] H. Faisst and B. Eckhardt, Travelling waves in pipe flow, Phys. Rev. Lett. **91**, 224502 (2003).

[16] F. A. Milinazzo and P. G. Saffman, Finite-amplitude steady waves in plane viscous shear flows, J. Fluid Mech. **160**, 281 (1985).

[17] H. Wedin, A. Bottaro, and M. Nagata, Three-dimensional traveling waves in a square duct, Phys. Rev. E **79**, 065305(R) (2009).

[18] H. Wedin, A. Bottaro, and M. Nagata, in *Advances in Turbulence XII*, Proceedings of the 12th EUROMECH European Turbulence Conference, edited by B. Eckhardt (Springer-Verlag, Berlin, Heidelberg, 2009), pp. 141–144.

[19] M. Uhlmann, G. Kawahara, and A. Pinelli, Traveling-waves consistent with turbulence-driven secondary flow in a square duct, Phys. Fluids **22**, 084102 (2010).

[20] S. Okino, M. Nagata, H. Wedin, and A. Bottaro, A new nonlinear vortex state in square duct flow, J. Fluid Mech. **657**, 413 (2010).

[21] G. Kawahara and S. Kida, Periodic motion embedded in plane Couette turbulence: Regeneration cycle and burst, J. Fluid Mech. **449**, 291 (2001).

[22] G. Kawahara, Laminarization of minimal plane Couette flow: Going beyond the basin of attraction of turbulence, Phys. Fluids **17**, 041702 (2005).

[23] G. Kawahara, S. Kida, and M. Nagata, in *Proceedings of the IUTAM Symposium on One Hundred Years of Boundary Layer Research*, edited by G. E. A. Meier, K. R. Sreenivasan, and H.-J. Heinemann (Springer, Netherlands, 2006), pp. 415–424.

[24] S. Cherubini, D. Palma, J. Robinet, and A. Bottaro, Edge states in a boundary layer, Phys. Fluids **23**, 051705 (2011).

[25] Y. Duguet, P. Schlatter, D. S. Henningson, and B. Eckhardt, Self-sustained localized structures in a boundary-layer flow, Phys. Rev. Lett. **108**, 044501 (2012).

[26] T. Kreilos, G. Veble, T. Schneider, and B. Eckhardt, Edge states for the turbulence transition in the asymptotic suction boundary layer, J. Fluid Mech. **726**, 100 (2013).

[27] T. Khapko, T. Kreilos, P. Schlatter, Y. Duguet, B. Eckhardt, and D. Henningson, Localized edge states in the asymptotic suction boundary layer, J. Fluid Mech. **717**, R6 (2013).

[28] G. Chandler and R. Kerswell, Invariant recurrent solutions embedded in a turbulent two-dimensional Kolmogorov flow, J. Fluid Mech. **722**, 554 (2013).

[29] M. Avila, F. Mellibovsky, N. Roland, and B. Hof, Streamwise-localized solutions at the onset of turbulence in pipe flow, Phys. Rev. Lett. **110**, 224502 (2013).

[30] M. Chantry, A. P. Willis, and R. R. Kerswell, Genesis of streamwise-localized solutions from globally periodic traveling waves in pipe flow, Phys. Rev. Lett. **112**, 164501 (2014).

[31] L. Hocking, Non-linear instability of the asymptotic suction velocity profile, Q. J. Mech. Appl. Math. **28**, 341 (1975).

[32] S. Cherubini, D. Palma, and J. Robinet, Non linear optimals in the asymptotic suction boundary layer: Transition thresholds and symmetry breaking, Phys. Fluids **27**, 034108 (2015).

[33] J. H. M. Fransson and P. H. Alfredsson, On the disturbance growth in an asymptotic suction boundary layer, J. Fluid Mech. **482**, 51 (2003).

[34] H. Schlichting, *Boundary-layer Theory*, 7th ed. (McGraw-Hill, New York, 1979).

[35] C. Gustavsson, Development of three-dimensional disturbances in boundary layers with suction, Master thesis, Luleå University of Technology, Sweden, 2000.

[36] J. Fransson, Flow control of boundary layers and wakes, Ph.D. thesis, Royal Institute of Technology, KTH Mechanics, 2003.

[37] J. Fransson and Corbett, Optimal linear growth in the asymptotic suction boundary layer, Eur. J. Mech. B/Fluids **22**, 259 (2003).

[38] O. Levin, E. Davidsson, and D. Henningson, Transition thresholds in the asymptotic suction boundary layer, Phys. Fluids **17**, 114104 (2005).

[39] E. Davidsson, Stability and transition in the suction boundary layer and other shear flows, Ph.D. thesis, Luleå University of Technology, Sweden, 2007.

[40] M. Innocentini, P. Sepulveda, and F. Ortega, Permeability, in *Cellular Ceramics. Structure, Manufacturing, Properties and Applications*, edited by M. Scheffler and P. Colombo (Wiley-VCH Verlag GmbH, Weinheim, Germany, 2005), pp. 313–341.

[41] F. Pluvinage, A. Kourta, and A. Bottaro, Instabilities in the asymptotic suction boundary layer over a permeable, compliant wall, Phys. Fluids **27**, 054104 (2015).

[42] R. Verzicco and P. Orlandi, A finite-difference scheme for the three-dimensional incompressible flows in cylindrical coordinates, J. Comp. Phys. **123**, 402 (1996).

[43] W. Rheinboldt and J. V. Burkardt, Algorithm 596: A program for a locally parameterized continuation process, ACM Trans. Math. Software **9**, 236 (1983).

[44] W. Rheinboldt and J. V. Burkardt, A locally parameterized continuation process, ACM Trans. Math. Software **9**, 215 (1983).

[45] P. J. Schmid and D. Henningson, in *Stability and Transition in Shear Flows* (Springer-Verlag, New York, 2001).

[46] J. Wang, J. Gibson, and F. Waleffe, Lower branch coherent states in shear flows: Transition and control, Phys. Rev. Lett. **98**, 204501 (2007).

[47] L. van Veen and G. Kawahara, Homoclinic tangle on the edge of shear turbulence, Phys. Rev. Lett. **107**, 114501 (2011).

[48] B. G. B. Klingmann, A. V. Boiko, K. J. A. Westin, V. V. Kozlov, and P. H. Alfredsson, Experiments on the stability of Tollmien-Schlichting waves, Eur. J. Mech. B/Fluids **12**, 493 (1993).